ACS NANO

www.acsnano.org

ARTICLE

Rapid Synthesis of Graphdiyne Films on Hydrogel at the Superspreading Interface for Antibacteria

Ya Kong, Xiaodan Li, Longwei Wang, Zixuan Zhang, Xueting Feng, Jing Liu, Chunying Chen,* Lianming Tong,* and Jin Zhang*

Cite This: *ACS Nano* 2022, 16, 11338–11345

Read Online

ACCESS | Metrics & More | Article Recommendations | Supporting Information

ABSTRACT: Graphdiyne (GDY), a two-dimensional (2D) carbon material with diacetylenic linkages (−C≡C−C≡C−) structures, has attracted enormous attention in various fields. However, the controlled synthesis of GDY films is still challenging because of the low alkyne coupling efficiency and out-of-plane growth. Here, we employed a highly efficient Cu(II)-N,N,N′,N′-tetramethylethylenediamine (Cu(II)-TMEDA) catalyst and constructed a superspreading liquid/liquid interface on a hydrogel for rapid and controllable synthesis of GDY thin films. GDY films with controllable thickness from 4 to 50 nm and large-scale uniform morphology can be prepared within 2 h at room temperature. The mechanism of growth was revealed to be a nucleation and in-plane extension process. Meanwhile, the as-grown GDY films showed excellent photothermal conversion efficiency, which induces the release of Cu(II) ions from the hydrogel and exhibits high efficiency in synergistic antibacteria.

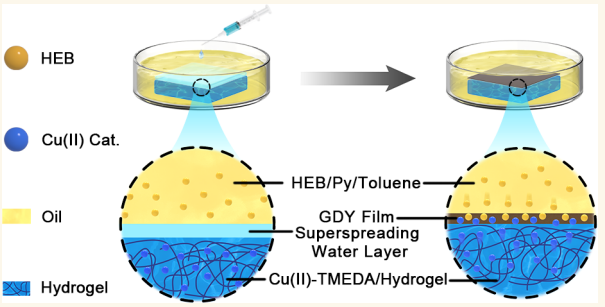

KEYWORDS: *graphdiyne, rapid synthesis, superspreading interface, photothermal, antibacteria*

Downloaded via PEKING UNIV on September 23, 2022 at 02:07:22 (UTC).
See https://pubs.acs.org/sharingguidelines for options on how to legitimately share published articles.

Graphdiyne (GDY) is a kind of two-dimensional (2D) carbon material with sp- and sp^2-hybridized carbon atoms. It has been reported that GDY is a semiconductor material with a natural band gap of 0.44−1.47 eV while possessing a high carrier mobility of 10^4 to 10^5 $cm^2 \cdot V^{-1} \cdot s^{-1}$ at room temperature.[1−3] At the same time, its unique chemical structure, that is, diacetylenic linkages (−C≡C−C≡C−), well-distributed pores, and large π-conjugated system, endows GDY extensive application prospects in many fields such as catalysis,[4,5] energy storage and conversion,[6,7] photoelectrical device,[8] and biomedicine.[9−12]

Since the successful preparation of GDY in 2010,[13] great efforts have been devoted into the controlled synthesis of GDY. Up until now, most of the wet chemical synthesis routes were through alkyne coupling reactions where hexaethynylbenzene (HEB) and copper were used as precursor and catalyst, respectively.[14] Nevertheless, a series of attendant challenges hinder the controllable synthesis of GDY films: (1) the low terminal alkyne coupling efficiencies of HEB lead to side reactions and a long reaction time (typically 24−72 h);[15] (2) the C−C bond rotation results in out-of-plane branches and three-dimensional growth;[16] (3) the thickness of GDY films is difficult to control because of the strong van der Waals' interaction. To overcome these problems, a series of approaches have been developed. Li et al. prepared GDY films with ∼1 μm thickness at 60 °C for 3 days using copper foils as catalyst and substrate.[13] Gao and Zhou both successfully prepared GDY films on graphene in 24 h at room temperature by employing $Cu(OAc)_2$ as catalysts.[17,18] Interface-confined methods at solid/liquid, liquid/liquid, or gas/liquid interfaces have already been widely adopted for the controlled growth of 2D polymeric materials.[19−22] Nishihara et al. reported a liquid/liquid interface-confined synthetic strategy to obtain GDY films with a thickness of 24 nm.[23] However, the growth of GDY films still lasts 24 h, and the terminal alkyne coupling efficiencies at room temperature need to be further improved.

In addition, it has been reported that GDY and its derivatives, such as graphdiyne oxide (GDYO), displayed great biosafety and compatibility for *in vivo* applications of

Received: May 21, 2022
Accepted: July 5, 2022
Published: July 8, 2022

© 2022 American Chemical Society

https://doi.org/10.1021/acsnano.2c04984
ACS Nano 2022, 16, 11338−11345

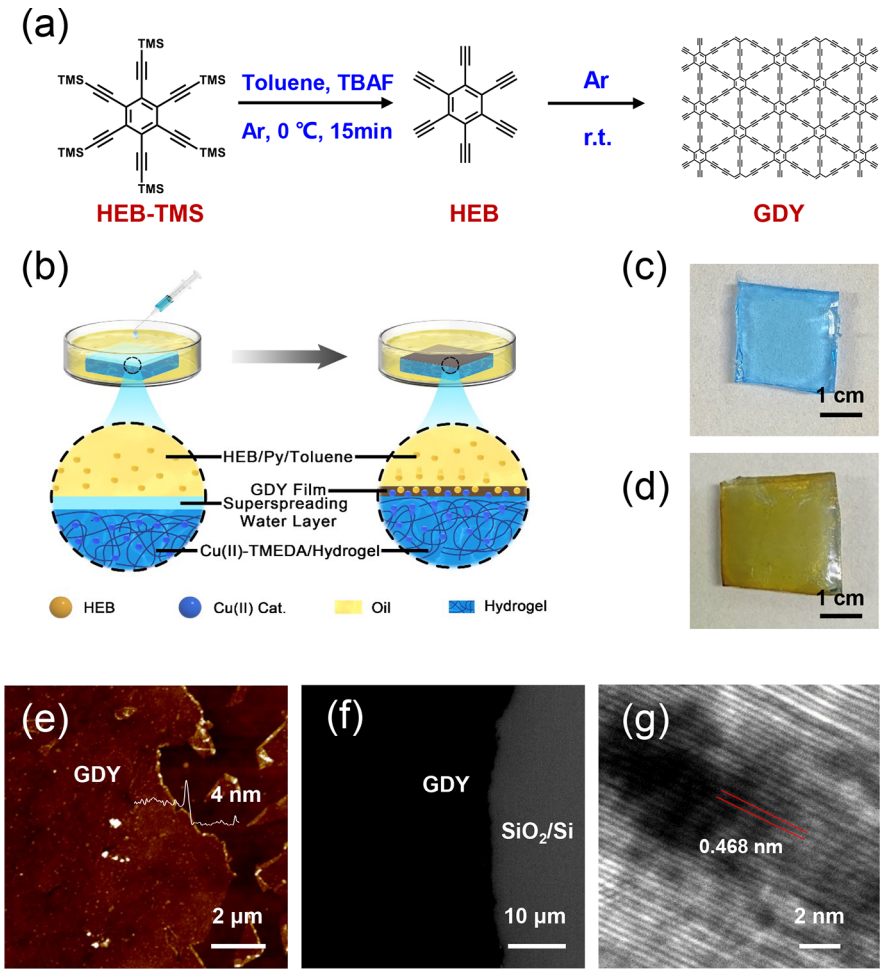

Figure 1. Synthetic process and characterization of graphdiyne (GDY) on a polyacrylamide (PAAM) hydrogel at the superspreading liquid/liquid interface. (a) Chemical structure of hexakis[(trimethylsilyl)ethynyl]benzene (HEB-TMS), hexaethynylbenzene (HEB), and the coupling reaction of the HEB molecule for the growth of GDY. TMS = $SiMe_3$. (b) Schematic illustration of the synthetic process. (c) Optical image of a PAAM hydrogel with Cu(II)-N,N,N′,N′-tetramethylethylenediamine (Cu(II)-TMEDA) catalyst. (d) Optical image of the GDY film on a PAAM hydrogel. (e) Typical atomic force microscope (AFM) image of the GDY film transferred onto a SiO_2/Si substrate, showing a thickness of ~4 nm. (f) Scanning electron microscopy (SEM) image of the GDY film transferred on a SiO_2/Si substrate. (g) High-resolution transmission electron microscopy (HRTEM) image of the GDY film.

antibacteria, biosensing and cancer therapy.[10,12] GDY and GDYO show antibacterial effects because of the generation of reactive oxygen species (ROS).[24] In particular, GDY and its complexes show excellent photothermal and photocatalytic performance enhancing the production of ROS.[25,26] Although the biomedical applications of GDY have been extensively studied, the use of GDY film with nanometer thickness was limited in the biomedical filed.

Here, we developed a general synthetic approach for rapid synthesis of GDY thin films within 2 h at room temperature. We employed a highly efficient Cu(II)-N,N,N′,N′-tetramethylethylenediamine (Cu(II)-TMEDA) catalyst, which greatly promotes the coupling efficiency, and constructed a superspreading liquid/liquid interface on the hydrogel, which controls the thickness of GDY film and realizes the slow release of catalyst for the alkyne coupling. Superspreading describes that a small droplet completely wets out on a substrate within tens of seconds[27] and has been successfully applied for the confined synthesis of a variety of polymer thin films.[28−30] Besides, functional hydrogels have been widespread applied as biocompatible scaffolds of cell therapy, drug delivery, artificial fiber, and soft electronics.[31−34]

By means of regulating the concentration of HEB monomers and the reaction time, the thickness of GDY films could be well controlled to be 4−50 nm. Through atomic force microscopy (AFM) characterization, the nucleation and in-plane expansion growth processes were discovered. The highly efficient terminal alkyne coupling reactions enhanced the density of nucleation and increased the growth rates, which was responsible for the rapid formation of films. The as-grown GDY films on the polyacrylamide (PAAM) hydrogel (GDY/PAAM hydrogel) could be directly used for antibacterial applications. The outstanding photothermal conversion effect of GDY films not only exerted antibacterial activity directly but also promoted the release of Cu(II) ions from the hydrogel, leading to 100% antibacterial effect. Overall, our work contributes to a successful approach for rapid synthesis of GDY nanofilms and manifests an excellent cooperative antibacteria for future application.

RESULTS AND DISCUSSION

Figure 1 panels a and b describe the schematic illustration of the synthetic process of GDY film on a PAAM hydrogel at the superspreading liquid/liquid interface. First, the mixed aqueous

https://doi.org/10.1021/acsnano.2c04984
ACS Nano 2022, 16, 11338−11345

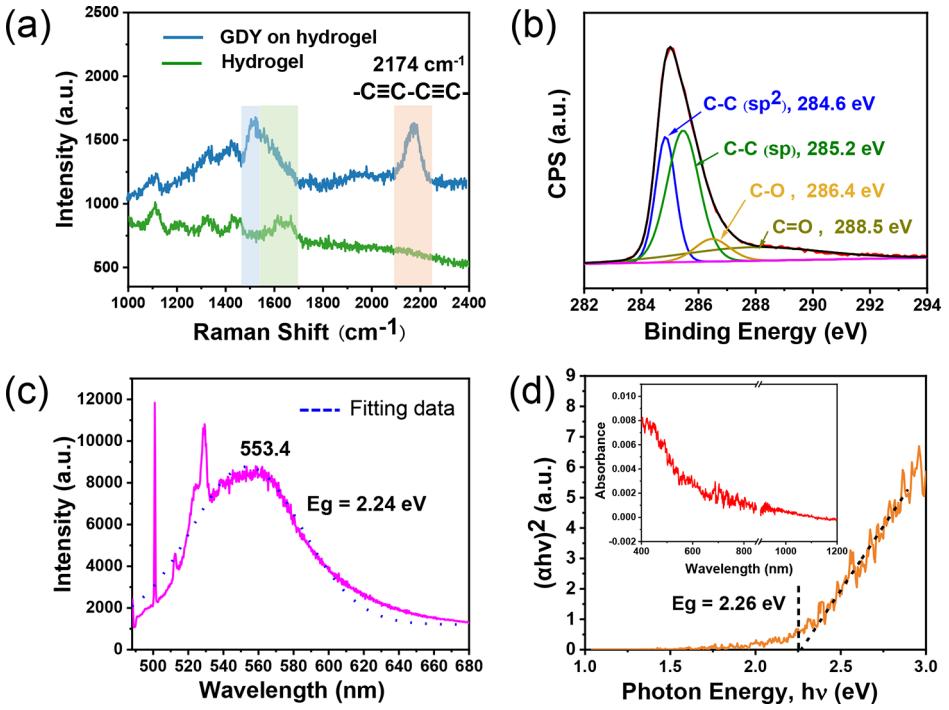

Figure 2. Spectroscopic characterization of as-grown GDY films. (a) Typical Raman spectra of a PAAM hydrogel (green line) and GDY film on PAAM hydrogel (blue line), excitation at 532 nm. (b) High-resolution core level X-ray photoelectron spectroscopy (XPS) spectrum of C 1s. (c) Photoluminescence (PL) spectrum of as-grown GDY film transferred onto the SiO_2/Si substrate. Blue dotted curve: fitting data. (d) Tauc plot of the GDY film corresponding to an optical bandgap of 2.26 eV .The inset is the UV−vis absorption spectrum of GDY film.

solution of $Cu(OAc)_2$ and acrylamide (AAM) could rapidly solidify into a PAAM hydrogel after the addition of TMEDA. Meanwhile, Cu(II) ions coordinated with TMEDA forming Cu(II)-TMEDA catalysts. Second, the PAAM hydrogel containing the Cu(II)-TMEDA catalysts was immersed in a toluene solution of HEB monomers. Because of the hydraulic pressure and the liquid-like properties of the hydrogel surfaces, 30 μL of water could spread out completely on the surface of the PAAM hydrogel to form a superspreading water layer.[28] Cu(II)-TMEDA catalysts released from the hydrogel into the water layer because of the concentration difference. Finally, thanks to the insolubility of HEB monomers in water and the low solubility of catalysts in toluene, monomers and catalysts could only meet at the water/toluene interface where the terminal alkyne coupling reactions occurred and GDY films were grown within only 2 h. On the one hand, because of the highly reaction efficiency of Cu(II)-TMEDA catalysts, the growth time of GDY films at room temperature is much shorter than those reported in literature.[17,18,23] On the other hand, the lower catalyst concentration in the water layer promotes the slow nucleation of GDY at the initial stage. Additionally, the PAAM hydrogel not only induces the formation of superspreading water layer and stores the Cu(II)-TMEDA catalysts but also serves as a quasi-solid substrate for supporting the GDY film. After the water layer was absorbed by the hydrogel, the GDY film formed on the surface of the hydrogel. Moreover, the equipment for continuous and large-scale production of GDY film was designed and used, as shown in Figure S1. Figure 1 panels c and d present the photos of the hydrogel before and after the reactions, respectively. On account of the storage of Cu(II)-TMEDA, PAAM hydrogel appears blue (Figure 1c). After reactions, an earthy yellow GDY film attached to the surface of the PAAM hydrogel (Figure 1d). By regulating the concentration of HEB monomers and the reaction time, the thickness of GDY films can be controlled to be 4−50 nm, as measured by atomic force microscopy (AFM) (Figure 1e and Figure S2). The shortest reaction time was only 2 h because of the highly efficient Cu(II)-TMEDA catalyst of the alkyne coupling reaction. Besides, because of the weaker interactions and different hydrophilicities between as-grown GDY films and the PAAM hydrogel, GDY films can be easily transferred to arbitrary substrates (Figure S3). The optical microscope (OM) images of GDY films on hydrogel and on SiO_2/Si substrate are displayed in Figure S4, which disclose the continuity of GDY films in a centimeter-sized area corresponding to the scanning electron microscopy (SEM) image (Figure 1f).

The morphology and crystallinity are further confirmed by transmission electron microscope (TEM). Energy-dispersive X-ray (EDX) spectroscopy elemental mapping images (Figure S5) show that the as-grown film is mainly composed of carbon. From the high-resolution TEM (HRTEM) image (Figure 1g), a lattice parameter of 0.468 nm is observed and is in good agreement with the (110) plane of GDY.[17] The electron diffraction pattern is shown in Figure S6. Comparing with the Raman spectrum of the PAAM hydrogel (Figure 2a green line), the Raman spectrum of the GDY film on the PAAM hydrogel exhibits three typical peaks in the range 1000−2400 cm^{-1}. According to the theoretical calculations,[35] the Y peak (centered at 2174 cm^{-1}) contains two components (Y′ and Y″) assigned to the in-phase and out-of-phase stretching modes of −C≡C−C≡C− triple bonds, respectively. The peaks centered at 1561 and 1524 cm^{-1} are defined as the G′ and G peaks, respectively, which are attributed to the vibration of sp^2-hybridized carbon atoms. The intensity of Y peak being comparable to the G peak represents the content of −C≡C−

https://doi.org/10.1021/acsnano.2c04984
ACS Nano 2022, 16, 11338−11345

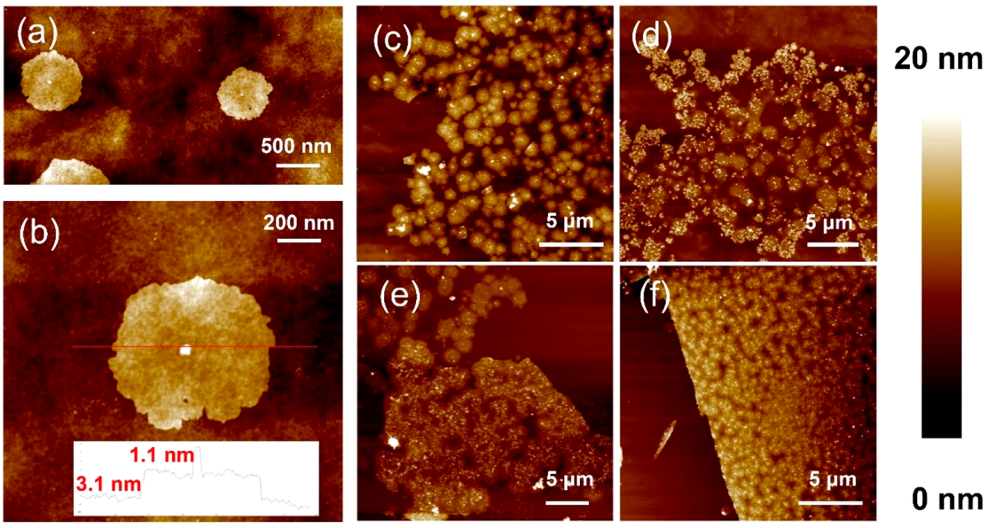

Figure 3. Typical atomic force microscope (AFM) images of GDY transferred onto SiO_2/Si substrate during the process of growth: (a,b) 0.5 h, (c) 2 h, (d) 6 h, (e) 12 h, (f) 18 h.

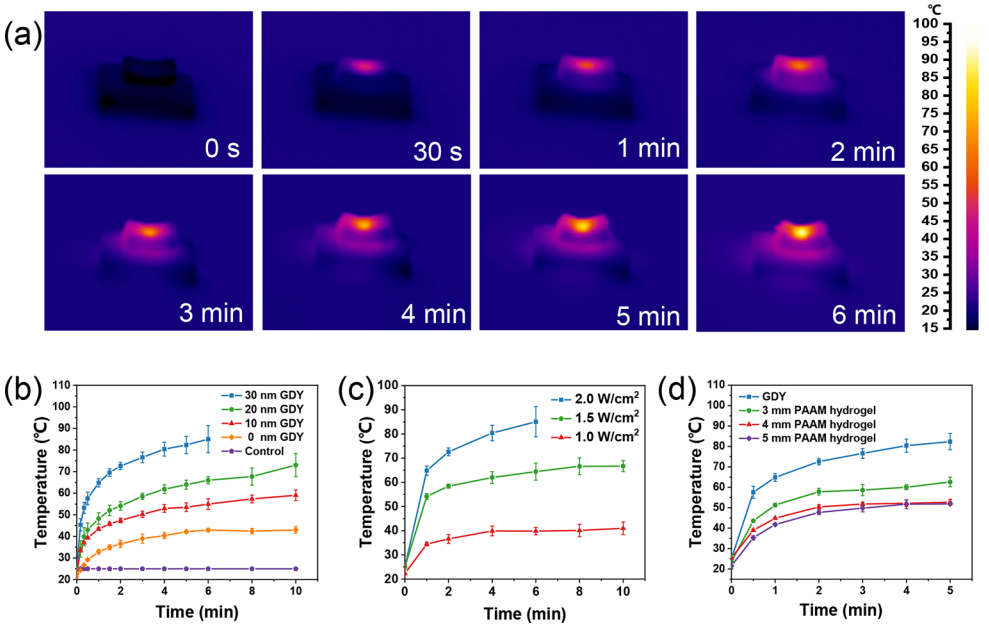

Figure 4. Photothermal effect of GDY films on PAAM hydrogel with Cu(II) ions. Laser: 808 nm. (a) Photothermal images of 30 nm GDY film on PAAM hydrogel with Cu(II) ions. (b) Temperature elevation of GDY films with different thicknesses on a PAAM hydrogel with Cu(II) ions upon NIR irradiation (2 W/cm^2). (c) Temperature elevation of GDY films on a PAAM hydrogel with Cu(II) ions upon different NIR irradiation powers. (d) Temperature elevation at the surface of GDY films and at the bottom of PAAM hydrogel of different thicknesses (2 W/cm^2).

C≡C− and further proves the high-efficiency of coupling reactions. X-ray photoelectron spectroscopy (XPS) survey scan indicates that the mainly composition of GDY films is carbon element (Figure S8). High-resolution core level XPS spectrum of C 1s (Figure 2b) can be deconvoluted into four peaks, including C—C (sp^2) at 284.6 eV, C—C (sp) at 285.2 eV, C—O at 286.4 eV, and C═O at 288.5 eV, respectively. The peak area ratio of the C—C (sp) and C—C (sp^2) is approximately 2, which originates from the number of sp- and sp^2-hybridized carbon atoms in GDY. In addition, the photoluminescence (PL) spectrum depicts a single emission peak at 553.4 nm with a photon energy of 2.24 eV (Figure 2c). Two sharp peaks at 500.6 and 512.5 nm are attributed to the first-order and second-order Raman active modes in back-scattering configuration for the SiO_2/Si substrate, respectively. The peaks at 524.3 and 529.3 nm are attributed to the G′ and G Raman active modes for GDY film corresponding to the Raman spectrum in Figure 2a and Figure S7. The 5 nm GDY film was transferred to a clear quartz glass substrate (Figure S3c) for optical absorption characterization. The UV−vis absorption spectrum of GDY film was shown in the inset of Figure 2d. On the basis of the semiconductor properties of GDY, the Tauc plot method[36] gives the optical bandgap of 2.26 eV (Figure 2d), which is close to the result of PL spectrum.

The copper-mediated acetylenic coupling reaction is the fundamental of GDY synthesis. Glaser coupling, Glaser−Hay coupling, and Eglinton coupling reactions have been adopted

https://doi.org/10.1021/acsnano.2c04984
ACS Nano 2022, 16, 11338−11345

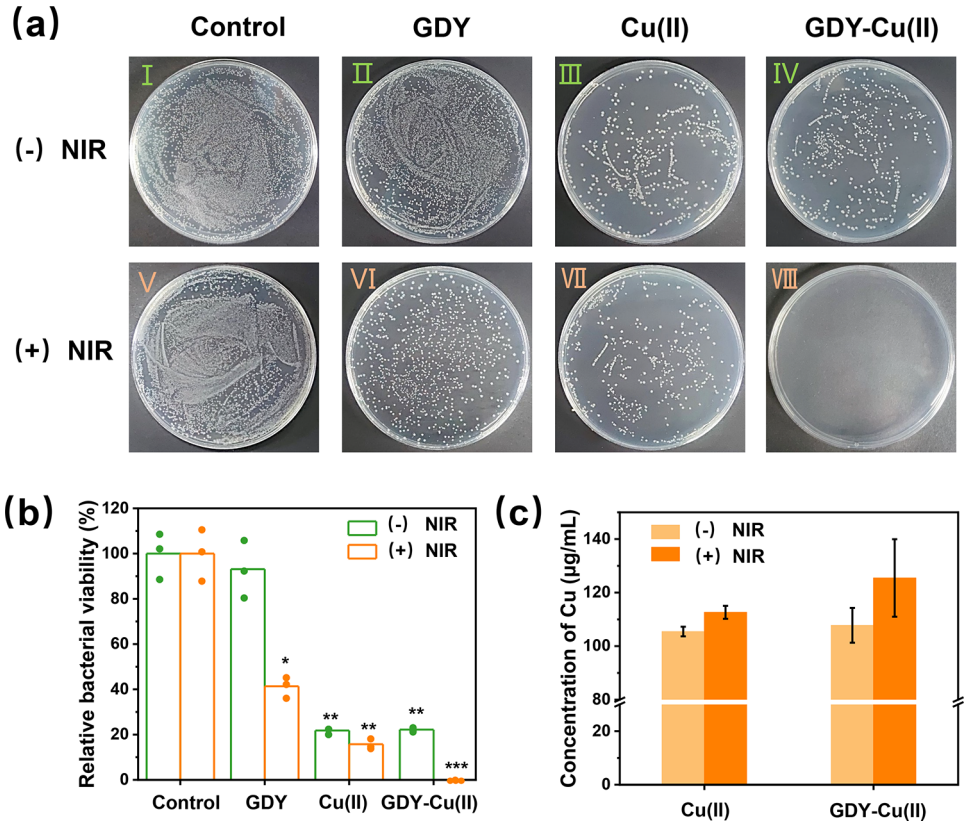

Figure 5. Assessment of antimicrobial capacity of GDY films. Laser: 808 nm, 2 W/cm^2. (a) Photographs of bacterial colonies formed by *E. coli* after exposure to (I) control, (II) GDY, (III) Cu(II), (IV) GDY-Cu(II), (V) control+NIR, (VI) GDY+NIR, (VII) Cu(II)+NIR, and (VIII) GDY-Cu(II)+NIR. (b) Relative bacteria viabilities of *E. coli* determined by plate count method. * $P < 0.001$, ** $P < 0.0002$, *** $P < 0.0001$ indicate significant differences compared to the control group without adding any substrate incubated for 20 min after NIR irradiation. (c) ICP-OES detection of Cu(II) ions release from hydrogels after 10 min of NIR radiation.

and modified for GDY preparation.[14,17,18] In the Glaser−Hay coupling reaction, CuCl serves as the main catalyst, and TMEDA is a bidentate ligand of Cu(I) as well as a base that could accelerate the reaction.[37] However, CuCl is an insoluble salt, in both aqueous and organic solvents, which limits its application. As for the Eglinton coupling, $Cu(OAc)_2$, a diffluent catalyst, with pyridine is adopted.[38] In the previous reports, the amount of pyridine is high, and it is unstable as a monotone ligand. Therefore, $Cu(OAc)_2$ with TMEDA was chosen in our work. To further illustrate the efficiency of the alkyne coupling reaction catalyst, we compared the coupling reaction efficiency of phenylacetylene using different catalysts, $Cu(OAc)_2$-TMEDA, $Cu(OAc)_2$-Py, CuCl-TMEDA, and $Cu(OAc)_2$, as shown in Figure S9. After 2 h of reaction at room temperature, CuCl-TMEDA is found to be the most efficient catalyst by detecting the concentration of the 1,4-diphenylbutadiyne via high performance liquid chromatography-mass spectrometry (HPLC-MS) analysis. $Cu(OAc)_2$ without ligand is the least effective catalyst. Indeed, we only need 2 h at room temperature to complete the synthesis of GDY films by adopting $Cu(OAc)_2$-TMEDA catalysts.

The superspreading liquid/liquid interface confines the synthesis of GDY and is indispensable to achieve GDY thin films. Figure S10 shows that the water spreads quickly over the surface of the PAAM hydrogel immersed at a depth of about 1 cm in toluene. Note that the contact angle of PAAM hydrogel in air is about 6° (Figure S11). Without the superspreading water layer, GDY could also grow on the surface of the PAAM hydrogel, but GDY films were discontinuous and GDY powders grew on the hydrogel, as shown in Figure S12.

To understand the growth mechanism of GDY films on the PAAM hydrogel, we characterized the morphology of GDY films at different stages during the growth with a relatively low monomer concentration (Figure 3 and Figure S13a−e). Interestingly, we found a few GDY grains with apparent nucleation centers, as shown in Figure 3a. GDY grains with near-hexagonal shapes are shown in Figure 3b. The AFM height profile in Figure 3b indicates the thickness of GDY grains and nucleation centers is 3.1 and 4.2 nm, respectively. As the reaction time increases, the in-plane extension of GDY grains coexists with multilayer growth (Figure 3c,d). It is anticipated that GDY grains grow in-plane until splice into the film (Figure 3e,f). The corresponding Raman spectra (Figure S13f) also confirm that the intensities of peaks at 1524, 1936, and 2174 cm^{-1} gradually increase as the nucleus grows and reach the highest until it grows into a film.

Because of the sp-hybridized carbon atoms and light absorption in a broad spectrum, GDY has been recently used as efficient photothermal agent in water desalination and biomedical fields.[39,40] To verify the near-infrared (NIR)-excitative photothermal effect of GDY/PAAM hydrogel, the temperature changes under NIR irradiation (808 nm) were monitored (Figure S14), and the results are shown in Figure 4. It is observed that, with the increase of GDY thickness, the heating rate increases and the maximum temperature grows (Figure 4b). The influence of the power density of NIR irradiation was investigated to optimize the photothermal

https://doi.org/10.1021/acsnano.2c04984
ACS Nano 2022, 16, 11338−11345

conversion performances (Figure 4c). The result reflects that the temperature of 30 nm GDY films can reach 85 °C after being irradiated for 6 min at a power density of 2 W/cm^2. By contrast, the temperature elevation of the control group (PAAM hydrogel without GDY and Cu(II) ions) is negligible. Furthermore, benefiting from the high thermal conductivity of GDY film, it only takes 1 min to drop from 70 to 30 °C after shutting off the NIR laser (Figure S15). We also investigated the heat transfer effect of 30 nm GDY films on the hydrogel with different thicknesses (Figure 4d). It is easy to understand that the thinner the hydrogel, the hotter it is at the bottom of the hydrogel after the same irradiation time. The temperature at the bottom of the hydrogel can reach 60 °C within 1 min. The temperature difference between the upper GDY film and the bottom of the hydrogel is 16.7 °C.

Taking advantage of the excellent photothermal effect of GDY films, the antibacterial ability was evaluated. The bacterial problem remains a worldwide challenge and the development of efficient antibacterial methods is urgent.[41] The antibacterial ability of *E. coli* was examined by the classical plate count method. Through the comparison of four groups: (I) control, (II) GDY, (III) Cu(II), and (IV) GDY-Cu(II) (Figure 5a), groups III and IV show relatively higher antibacterial activity, which is attributed to the release of Cu(II) ions from the hydrogel. Compared to (−) NIR groups I−IV, the groups (VI) GDY+NIR, (VII) Cu(II)+NIR, and (VIII) GDY-Cu(II)+NIR possessed enhanced antimicrobial activity after NIR irradiation. Among these, group VIII shows extremely efficient sterilizing effect (an inhibition rate of up to near 100%). Figure 5b shows the detailed statistics of sterilization. The disinfection efficiency of the control group is basically 0% and, moreover, 7%, 79%, and 78% for groups II−IV, respectively. In contrast, the disinfection efficiencies of groups VI−VIII are improved to 59%, 85%, and 100% after NIR irradiation. This result is also verified in the bacterial live/dead assay. As shown in Figure S16, all bacteria die in the GDY-Cu(II)+NIR group, whereas some bacteria survive in Cu(II) and the Cu(II)+NIR group and most bacteria survive in the GDY+NIR group and PBS buffer groups. The morphological changes of bacteria after GDY-Cu(II) treatment were visualized by SEM. As reported in literature,[26] the bacteria remain integral cell membranes in PBS buffer whereas bacteria become aggregated and surfaces appear visibly rough and crumpled after treatment (Figure S16b). To further decipher the antibacterial behavior, the concentration of Cu(II) ions released from the hydrogels into the PBS was detected using an inductively coupled plasma-atomic emission spectrometer (ICP-OES) (Figure 5c). As expected, under the NIR irradiation, the Cu(II) ion release concentration of group VIII was the highest (125.5 μg/mL). The results further verify that the enhanced Cu(II) ion release is attributed to the excellent photothermal effect of GDY films in accord with the best bactericidal effect. The two actions, the photothermal effect and the Cu(II) ion release, complement each other in a bid to a powerful antibacterial ability.

CONCLUSION

In conclusion, we employed a highly efficienct Cu(II)-TMEDA catalyst for acetylenic coupling reaction and constructed a superspreading liquid/liquid interfacial-confined system for rapid and controllable synthesis of GDY films. Through the coupling reactions of HEB monomers within water/toluene interface, GDY films with thicknesses from 4 to 50 nm and large-scale uniform topography can be obtained on the surface of the PAAM hydrogel. The growth time was only 2 h at room temperature. Meanwhile, the stages of nucleation and in-plane extension growth were also detected, which demonstrated the GDY film growth process. What's more, GDY films on hydrogel could not only be easily transferred onto arbitrary substrates but also be directly applied for a synergistic antibacterial system because of the excellent photothermal conversion efficiency of GDY film and the improvement of metal-ions-releasing capability. This work provides an avenue for rapid synthesis of GDY films and exhibits an excellent synergistic antimicrobial effect for future applications.

METHODS

Preparation of PAAM Hydrogel with Cu(II)-TMEDA Catalyst. Acrylamide (AAM) (7.5 g), *N*,*N*′-methylenebis(acrylamide) (MBAAM) (0.15 g), ammonium persulfate (APS) (0.15 g), and cupric acetate monohydrate ($Cu(OAc)_2 \cdot H_2O$) (0.1 g) dissolve in 50 mL of distilled water. 30 mL of the aqueous solution was added into a 100 mm glass petri dish with a 300 nm SiO_2/Si wafer. The addition of TMEDA (90 μL) promotes radical polymerization of the aqueous solution and complexation with copper ions. The obtained PAAM hydrogel with Cu(II)-TMEDA catalyst were dipped in an aqueous solution of Cu(II)-TMEDA at the same concentration staying overnight to fully swollen.

Synthesis of GDY Films. The cut PAAM hydrogels were immersed in toluene solution of HEB monomers keeping the surface of the hydrogel at least 1 cm from the liquid level. Then, 30 μL of water was dropped on the hydrogel surface and formed a superspreading water layer. After reaction under an argon atmosphere at room temperature, the GDY film was successfully prepared on the surface of the PAAM hydrogel. By controlling the concentration of HEB-TMS and reaction time, the thickness of the GDY film ranging from 4 to 50 nm could be regulated. For example, a 4 nm thick film was obtained by using 0.17 mg/mL of HEB-TMS for 2 h, and 10, 30, and 50 nm GDY film was prepared by using 0.5 mg/mL of HEB-TMS for 6, 12, and 24 h, respectively.

Antibacterial Activity. Bacteria were incubated separately with eight different groups: (I) control, (II) GDY, (III) Cu(II), (IV) GDY-Cu(II), (V) control+NIR, (VI) GDY+NIR, (VII) Cu(II)+NIR, and (VIII) GDY-Cu(II)+NIR. Hydrogels (1 × 1 cm^2) were placed in a 3.48 nm Petri dish containing 2 mL of PBS. An 808 nm laser (2 W/cm^2) was used as the near-infrared (NIR) source. The bacterial concentration was measured at laser irradiation for 10 min and at rest for 20 min using standard spread plating techniques. Each sample was gradiently diluted, and each dilution in triplicate was plated onto the trypticase soy agar culture medium and incubated at 37 °C for 18 h. The experiments for the antibacterial performance were conducted in duplicate. The bacteria survival rate was calculated using the following equation:

$$\% \text{ survival} = C/C_0 \times 100\%$$

where C is the terminal concentration of bacteria and C_0 is the concentration at $t = 0$ of the experiments.

ASSOCIATED CONTENT

Supporting Information

The Supporting Information is available free of charge at https://pubs.acs.org/doi/10.1021/acsnano.2c04984.

Scheme of equipment for continuous and large-scale preparation and optical image of large-scale sample; transfer process; OM images, AFM images, TEM images, SAED pattern, Raman spectrum, XPS spectrum, and contact angle measurement of GDY films; characterization of terminal alkyne coupling reaction efficiency catalyzed by different catalysts; process of water spreading on the surface of a PAAM hydrogel immersed

https://doi.org/10.1021/acsnano.2c04984
ACS Nano 2022, 16, 11338−11345

in toluene; photothermal response measurements; fluorescence images and SEM images of live/dead of *E. coli* (PDF)

AUTHOR INFORMATION

Corresponding Authors

Chunying Chen − *CAS Key Laboratory for Biomedical Effects of Nanomaterials and Nanosafety and CAS Center for Excellence in Nanoscience, National Center for Nanoscience and Technology of China, Beijing 100190, P. R. China;* orcid.org/0000-0002-6027-0315; Email: chenchy@nanoctr.cn

Lianming Tong − *Center for Nanochemistry, Beijing Science and Engineering Center for Nanocarbons, Beijing National Laboratory for Molecular Sciences, College of Chemistry and Molecular Engineering, Peking University, Beijing 100871, P. R. China;* orcid.org/0000-0001-7771-4077; Email: tonglm@pku.edu.cn

Jin Zhang − *Center for Nanochemistry, Beijing Science and Engineering Center for Nanocarbons, Beijing National Laboratory for Molecular Sciences, College of Chemistry and Molecular Engineering, Peking University, Beijing 100871, P. R. China;* orcid.org/0000-0003-3731-8859; Email: jinzhang@pku.edu.cn

Authors

Ya Kong − *Center for Nanochemistry, Beijing Science and Engineering Center for Nanocarbons, Beijing National Laboratory for Molecular Sciences, College of Chemistry and Molecular Engineering, Peking University, Beijing 100871, P. R. China*

Xiaodan Li − *Academy for Advanced Interdisciplinary Studies, Peking University, Beijing 100871, P. R. China; CAS Key Laboratory for Biomedical Effects of Nanomaterials and Nanosafety and CAS Center for Excellence in Nanoscience, National Center for Nanoscience and Technology of China, Beijing 100190, P. R. China*

Longwei Wang − *CAS Key Laboratory for Biomedical Effects of Nanomaterials and Nanosafety and CAS Center for Excellence in Nanoscience, National Center for Nanoscience and Technology of China, Beijing 100190, P. R. China*

Zixuan Zhang − *Center for Nanochemistry, Beijing Science and Engineering Center for Nanocarbons, Beijing National Laboratory for Molecular Sciences, College of Chemistry and Molecular Engineering, Peking University, Beijing 100871, P. R. China*

Xueting Feng − *Center for Nanochemistry, Beijing Science and Engineering Center for Nanocarbons, Beijing National Laboratory for Molecular Sciences, College of Chemistry and Molecular Engineering, Peking University, Beijing 100871, P. R. China*

Jing Liu − *CAS Key Laboratory for Biomedical Effects of Nanomaterials and Nanosafety and CAS Center for Excellence in Nanoscience, National Center for Nanoscience and Technology of China, Beijing 100190, P. R. China;* orcid.org/0000-0002-8740-4600

Complete contact information is available at: https://pubs.acs.org/10.1021/acsnano.2c04984

Author Contributions

Y. Kong, L. Wang, J. Zhang, C. Chen, L. Tong, and J. Liu conceived and planned the project. Y. Kong, X. Li, and L. Wang conducted experiments and carried out data analysis. All the authors discussed the results and helped in writing the manuscript.

Funding

This work was financially supported by the Ministry of Science and Technology of China (2018YFA0703502 and 2016YFA0200100), the National Natural Science Foundation of China (Grant Nos. 52021006, 51720105003, 21790052, 21974004), the Strategic Priority Research Program of CAS (XDB36030100), and the Beijing National Laboratory for Molecular Sciences (BNLMS-CXTD-202001).

Notes

The authors declare no competing financial interest.

ACKNOWLEDGMENTS

We thank Y. Liu, Y. Zhang, N. Yan, L. Lai, and B. Cheng for their help and discussion.

REFERENCES

(1) Narita, N.; Nagai, S.; Suzuki, S.; Nakao, K. Optimized Geometries and Electronic Structures of Graphyne and Its Family. *Phys. Rev. B* **1998**, *58*, 11009−11014.

(2) Long, M.; Tang, L.; Wang, D.; Li, Y.; Shuai, Z. Electronic Structure and Carrier Mobility in Graphdiyne Sheet and Nanoribbons: Theoretical Predictions. *ACS Nano* **2011**, *5*, 2593−2600.

(3) Zheng, Q.; Luo, G.; Liu, Q.; Qu, R.; Zheng, J.; Tang, K.; Gao, Z.; Nagase, S.; Lu, J. Structural and Electronic Properties of Bilayer and Trilayer Graphdiyne. *Nanoscale* **2012**, *4*, 3990−3996.

(4) Qi, H.; Yu, P.; Wang, Y.; Han, G.; Liu, H.; Yi, Y.; Li, Y.; Mao, L. Graphdiyne Oxides as Excellent Substrate for Electroless Deposition of Pd Clusters with High Catalytic Activity. *J. Am. Chem. Soc.* **2015**, *137*, 5260−5263.

(5) Li, J.; Gao, X.; Jiang, X.; Li, X.; Liu, Z.; Zhang, J.; Tung, C.; Wu, L. Graphdiyne: A Promising Catalyst-Support To Stabilize Cobalt Nanoparticles for Oxygen Evolution. *ACS Catal.* **2017**, *7*, 5209−5213.

(6) Wang, N.; He, J.; Wang, K.; Zhao, Y.; Jiu, T.; Huang, C.; Li, Y. Graphdiyne-Based Materials: Preparation and Application for Electrochemical Energy Storage. *Adv. Mater.* **2019**, *31*, 1803202.

(7) Chen, X.; Jiang, X.; Yang, N. Graphdiyne Electrochemistry: Progress and Perspectives. *Small* **2022**, *18*, 2201135.

(8) Guo, J.; Shi, R.; Wang, R.; Wang, Y.; Zhang, F.; Wang, C.; Chen, H.; Ma, C.; Wang, Z.; Ge, Y.; Song, Y.; Luo, Z.; Fan, D.; Jiang, X.; Xu, J.; Zhang, H. Graphdiyne-Polymer Nanocomposite as a Broadband and Robust Saturable Absorber for Ultrafast Photonics. *Laser & Photon. Rev.* **2020**, *14*, 1900367.

(9) Wang, C.; Yu, P.; Guo, S.; Mao, L.; Liu, H.; Li, Y. Graphdiyne Oxide as a Platform for Fluorescence Sensing. *Chem. Commun.* **2016**, *52*, 5629−5632.

(10) Li, S.; Chen, Y.; Liu, H.; Wang, Y.; Liu, L.; Lv, F.; Li, Y.; Wang, S. Graphdiyne Materials as Nanotransducer for *in Vivo* Photoacoustic Imaging and Photothermal Therapy of Tumor. *Chem. Mater.* **2017**, *29*, 6087−6094.

(11) Guo, J.; Guo, M.; Wang, F.; Jin, W.; Chen, C.; Liu, H.; Li, Y. Graphdiyne: Structure of Fluorescent Quantum Dots. *Angew. Chem., Int. Ed.* **2020**, *59*, 16712−16716.

(12) Liu, J.; Chen, C.; Zhao, Y. Progress and Prospects of Graphdiyne-Based Materials in Biomedical Applications. *Adv. Mater.* **2019**, *31*, 1804386.

(13) Li, G.; Li, Y.; Liu, H.; Guo, Y.; Li, Y.; Zhu, D. Architecture of Graphdiyne Nanoscale Films. *Chem. Commun.* **2010**, *46*, 3256−3258.

(14) Kong, Y.; Li, J.; Zeng, S.; Yin, C.; Tong, L.; Zhang, J. Bridging the Gap between Reality and Ideality of Graphdiyne: The Advances of Synthetic Methodology. *Chem.* **2020**, *6*, 1933−1951.

(15) Li, X.; Zhang, H.; Chi, L. On-Surface Synthesis of Graphyne-Based Nanostructures. *Adv. Mater.* **2019**, *31* (42), No. e1804087.

(16) Sakamoto, J.; van Heijst, J.; Lukin, O.; Schlüter, A. Two-Dimensional Polymers: Just a Dream of Synthetic Chemists? *Angew. Chem., Int. Ed.* **2009**, *48*, 1030−1069.
(17) Gao, X.; Zhu, Y. H.; Yi, D.; Zhou, J.; Zhang, S.; Yin, C.; Ding, F.; Zhang, S. Q.; Yi, X.; Wang, J.; Tong, L.; Han, Y.; Liu, Z.; Zhang, J. Ultrathin Graphdiyne Film on Graphene through Solution-Phase Van Der Waals Epitaxy. *Sci. Adv.* **2018**, *4* (7), No. eaat6378.
(18) Zhou, J.; Xie, Z.; Liu, R.; Gao, X.; Li, J.; Xiong, Y.; Tong, L.; Zhang, J.; Liu, Z. Synthesis of Ultrathin Graphdiyne Film Using a Surface Template. *ACS Appl. Mater. Interfaces* **2019**, *11*, 2632−2637.
(19) Dmitriev, A.; Spillmann, H.; Lin, N.; Barth, J.; Kern, K. Modular Assembly of Two-Dimensional Metal-Organic Coordination Networks at a Metal Surface. *Angew. Chem., Int. Ed.* **2003**, *42*, 2670−2673.
(20) Makiura, R.; Motoyama, S.; Umemura, Y.; Yamanaka, H.; Sakata, O.; Kitagawa, H. Surface Nano-Architecture of a Metal-Organic Framework. *Nat. Mater.* **2010**, *9*, 565−571.
(21) Rodenas, T.; Luz, I.; Prieto, G.; Seoane, B.; Miro, H.; Corma, A.; Kapteijn, F.; Llabres, I.; Gascon, J. Metal-Organic Framework Nanosheets in Polymer Composite Materials for Gas Separation. *Nat. Mater.* **2015**, *14*, 48−55.
(22) Dai, W.; Shao, F.; Szczerbiński, J.; McCaffrey, R.; Zenobi, R.; Jin, Y.; Schlüter, A. D.; Zhang, W. Synthesis of a Two-Dimensional Covalent Organic Monolayer through Dynamic Imine Chemistry at the Air/Water Interface. *Angew. Chem., Int. Ed.* **2016**, *55*, 213−217.
(23) Matsuoka, R.; Sakamoto, R.; Hoshiko, K.; Sasaki, S.; Masunaga, H.; Nagashio, K.; Nishihara, H. Crystalline Graphdiyne Nanosheets Produced at a Gas/Liquid or Liquid/Liquid Interface. *J. Am. Chem. Soc.* **2017**, *139*, 3145−3152.
(24) Zhu, Z.; Bai, Q.; Li, S.; Li, S.; Liu, M.; Du, F.; Sui, N.; Yu, W. Antibacterial Activity of Graphdiyne and Graphdiyne Oxide. *Small* **2020**, *16*, 2001440.
(25) Wang, R.; Shi, M.; Xu, F.; Qiu, Y.; Zhang, P.; Shen, K.; Zhao, Q.; Yu, J.; Zhang, Y. Graphdiyne-Modified TiO_2 Nanofibers with Osteoinductive and Enhanced Photocatalytic Antibacterial Activities to Prevent Implant Infection. *Nat. Commun.* **2020**, *11*, 4465.
(26) Bai, Q.; Liang, M.; Wu, W.; Zhang, C.; Li, X.; Liu, M.; Yang, D.; Yu, W.; Hu, Q.; Wang, L.; Du, F.; Sui, N.; Zhu, Z. Plasmonic Nanozyme of Graphdiyne Nanowalls Wrapped Hollow Copper Sulfide Nanocubes for Rapid Bacteria-Killing. *Adv. Funct. Mater.* **2022**, *32*, 2112683.
(27) Venzmer, J. Superspreading - 20 Years of Physicochemical Research. *Curr. Opin. Colloid Interface Sci.* **2011**, *16*, 335−343.
(28) Zhang, P.; Zhang, F.; Zhao, C.; Wang, S.; Liu, M.; Jiang, L. Superspreading on Immersed Gel Surfaces for the Confined Synthesis of Thin Polymer Films. *Angew. Chem., Int. Ed.* **2016**, *55*, 3615−3619.
(29) Kan, X.; Wang, D.; Pan, Q.; Wang, Y.; Xiao, Y.; Liu, J.; Zhao, Y.; Li, Z. Confined Interfacial Synthesis of Highly Crystalline and Ultrathin Graphdiyne Films and Their Applications for N_2 Fixation. *Chem.—Eur. J.* **2020**, *26*, 7801−7807.
(30) Hao, Q.; Zhao, C.; Sun, B.; Lu, C.; Liu, J.; Liu, M.; Wan, L.; Wang, D. Confined Synthesis of Two-Dimensional Covalent Organic Framework Thin Films within Superspreading Water Layer. *J. Am. Chem. Soc.* **2018**, *140*, 12152−12158.
(31) Lin, W.; Kluzek, M.; Iuster, N.; Shimoni, E.; Kampf, N.; Goldberg, R.; Klein, J. Cartilage-Inspired, Lipid-Based Boundary-Lubricated Hydrogels. *Science* **2020**, *370*, 335−338.
(32) Liu, C.; Morimoto, N.; Jiang, L.; Kawahara, S.; Noritomi, T.; Yokoyama, H.; Mayumi, K.; Ito, K. Tough Hydrogels with Rapid Self-Reinforcement. *Science* **2021**, *372*, 1078−1081.
(33) Li, Z.; Li, G.; Xu, J.; Li, C.; Han, S.; Zhang, C.; Wu, P.; Lin, Y.; Wang, C.; Zhang, J.; Li, X. Hydrogel Transformed from Nanoparticles for Prevention of Tissue Injury and Treatment of Inflammatory Diseases. *Adv. Mater.* **2022**, *34*, 2109178.
(34) Wang, C.; Liu, Y.; Qu, X.; Shi, B.; Zheng, Q.; Lin, X.; Chao, S.; Wang, C.; Zhou, J.; Sun, Y.; Mao, G.; Li, Z. Ultra-Stretchable and Fast Self-Healing Ionic Hydrogel in Cryogenic Environments for Artificial Nerve Fiber. *Adv. Mater.* **2022**, *34*, 2105416.
(35) Zhang, S.; Wang, J.; Li, Z.; Zhao, R.; Tong, L.; Liu, F.; Zhang, J.; Liu, Z. Raman Spectra and Corresponding Strain Effects in Graphyne and Graphdiyne. *J. Phys. Chem. C* **2016**, *120*, 10605−10613.
(36) Fox, M. *Optical Properties of Solids*; Oxford University Press: New York, 2001.
(37) Fomina, L.; Vazquez, B.; Tkatchouk, E.; Fomine, S. The Glaser Reaction Mechanism. A DFT Study. *Tetrahedron* **2002**, *58*, 6741−6747.
(38) Eglinton, G.; Galbralth, A. Macrocyclic Acetylenic Compounds. Part I. Cyclotetradeca-1:3-diyne and Related Compounds. *J. Chem. Soc.* **1959**, 889−896.
(39) Huang, C.; Li, Y.; Wang, N.; Xue, Y.; Zuo, Z.; Liu, H.; Li, Y. Progress in Research into 2D Graphdiyne-Based Materials. *Chem. Rev.* **2018**, *118*, 7744−7803.
(40) Gao, X.; Ren, H.; Zhou, J.; Du, R.; Yin, C.; Liu, R.; Peng, H.; Tong, L.; Liu, Z.; Zhang, J. Synthesis of Hierarchical Graphdiyne-Based Architecture for Efficient Solar Steam Generation. *Chem. Mater.* **2017**, *29*, 5777−5781.
(41) Pang, X.; Xiao, Q.; Cheng, Y.; Ren, E.; Lian, L.; Zhang, Y.; Gao, H.; Wang, X.; Leung, W.; Chen, X.; Liu, G.; Xu, C. Bacteria-Responsive Nanoliposomes as Smart Sonotheranostics for Multidrug Resistant Bacterial Infections. *ACS Nano* **2019**, *13* (2), 2427−2438.

Recommended by ACS

Photocatalytic Hydrogels with a High Transmission Polymer Network for Pollutant Remediation
Thomas Kuckhoff, Calum T. J. Ferguson, *et al.*
NOVEMBER 21, 2021
CHEMISTRY OF MATERIALS
READ

Stimuli-Responsive Structural Colored Gel That Exhibits the Three Primary Colors of Light by Using Multiple Photonic Band Gaps Acquired from Photonic Balls
Yumiko Ohtsuka, Yukikazu Takeoka, *et al.*
NOVEMBER 18, 2020
ACS APPLIED MATERIALS & INTERFACES
READ

Light-Driven Expansion of Spiropyran Hydrogels
Chuang Li, Samuel I. Stupp, *et al.*
APRIL 24, 2020
JOURNAL OF THE AMERICAN CHEMICAL SOCIETY
READ

Spiropyran Photoisomerization Dynamics in Multiresponsive Hydrogels
Amos Meeks, Joanna Aizenberg, *et al.*
DECEMBER 29, 2021
JOURNAL OF THE AMERICAN CHEMICAL SOCIETY
READ

Get More Suggestions >

https://doi.org/10.1021/acsnano.2c04984
ACS Nano 2022, 16, 11338−11345